Uniaxial strain softening of concrete

Eindhoven University of Technology
Department of Structural Design And Engineering

UNIAXIAL STRAIN SOFTENING OF CONCRETE

Influence of Specimen Size and Boundary Shear

Tests Carried out for RILEM Commitee 148ssc:
"Strain Softening of Concrete"

Report BKO94.09 July 1994
ir. H.J.G.M. van Geel

Contents.

1. Introduction.

The tests described in this report are carried out in april and may of 1994. The new RILEM-Committee *Strain Softening of Concrete* (148ssc) is now aiming at gathering a great number of data to obtain a clear and systematic overview of strain softening of concrete in uniaxial compression and the factors influencing this phenomenon, in particular the way in which the tests are carried out. The major goal of the committee is to establish a standard test method for the determination of strain-softening behaviour of concrete in uniaxial compression.
Therefore a round robin test is set up in which the following parameters are examined: friction between loading platen and specimen, allowable rotations of the loading platen, the gauge length of the control LVDT, the shape and size of the concrete test specimen, the stiffness of the testing machine, the type of feed-back signal and the concrete composition and quality. In the present experiments the main factors of interest are the friction between loading platen and specimen and the size of the specimens.
From the viewpoint of the Eindhoven University of Technology these tests are part of an exhaustive research into the softening behaviour of concrete. In 1980, dr.ir. J.G.M. van Mier started this research by building a loading apparatus capable of applying true triaxial stress states on cubical specimens, after which he carried out a great amount of uniaxial, biaxial and triaxial softening tests. In 1986, dr.ir. R.A. Vonk continued the research project, taking a closer look at some significant parameters on uniaxial strain softening, like boundary shear, size effect and nonuniform deformations. Furthermore he developed a micromechanical model for strain softening of concrete which appeared to be capable of simulating the behaviour observed in experiments quite well. In 1993, the influence of concrete composition was examined in uniaxial softening tests by Darek Stys.
At the moment, the author of this report (engaged in the subject since 1993) is preparing a multiaxial test series as a continuation of the Eindhoven research. Since 1992 ir. J.P.W. Bongers is working on a numerical model at the macroscopic level. At the moment the numerical and experimental research is carried out in close cooperation. The survey of literature at the end of this report gives an overview of the research carried out at the Eindhoven University of Technology.

This research is partly supported by the Dutch Technology Foundation (STW) and supervised by prof.dr.ir. H.S. Rutten and ir. H.J. Fijneman. The tests are carried out in the Pieter van Musschenbroek Laboratory at Eindhoven University of Technology. Ing. M.A.C.M. Ceelen supported the laboratory work. The author acknowledges the support of abovementioned persons and STW.

ir. Erik van Geel,
July 1994.

2. Experimental technique.

In figure 1 the test setup is presented schematically. In the following sections a more detailed description of the several components will be given.

2.1. Loading apparatus.

All tests were carried out using the triaxial loading apparatus of the Eindhoven University of Technology, previously used by Van Mier [1984], Vonk [1992] and Stys [1994]. The apparatus consists of three independent loading axes, able to apply true triaxial stress states on cubical specimens. In the present uniaxial tests only one loading axis was in operation.
The loading apparatus is hung in a steel frame by means of steel cables. The compressive capacity of the apparatus is 2000 kN. Its rotational stiffness was found to be about $1.35*10^9$ Nm/rad [Vonk,1992, Stys,1994]. From top to bottom the loading axis consists of the following primary elements:
1. A hydraulic actuator, controlled by an external electric current. Inside this actuator a control-lvdt with a range of ±100 mm is mounted.
2. A hinge. It is possible to fix the hinge by means of steel bolts. Before the test program was carried out, the hinge was removed from the loading apparatus to check the amount and distribution of grease within the hinge.
3. Hardened (approximately 50 Rc) and polished (Ra≈0.04 μm) steel loading platens (97x97 mm²). The loading platens (Dominal PVS44 Steel, DIN-code X45NiCrMo4) were unused at the start of the present test program.
4. Two control-lvdt's (range ±10 mm) positioned diagonally opposite to each other at a fixed distance of the loading platen.
5. A load cell to record the load applied by the actuator. The load cell consists of a steel cylinder upon which four strain gauges are attached and which is covered by a second steel cylinder to protect the gauges. Before the test program was carried out, the load cell was recalibrated.

2.2. Test control.

The main component of the test control circuit is the Schenck S59 servo controller. This device controls the magnitude of electric current sent to the actuator's valve, which depends on the difference between the actual displacement and the displacement command value and of the chosen control parameters. The actual displacement value is measured by means of the two control-lvdt's (or the control-lvdt inside the actuator). The displacement command value is generated by an external function generator (MTS 418-91 Microprofiler), which forces the servo controller to apply a constant displacement rate of 1 μm/s. This displacement rate could be checked continuously by means of a Keithley 175 Autoranging Multimeter (1 μm/s ≡ 1 mV/s).

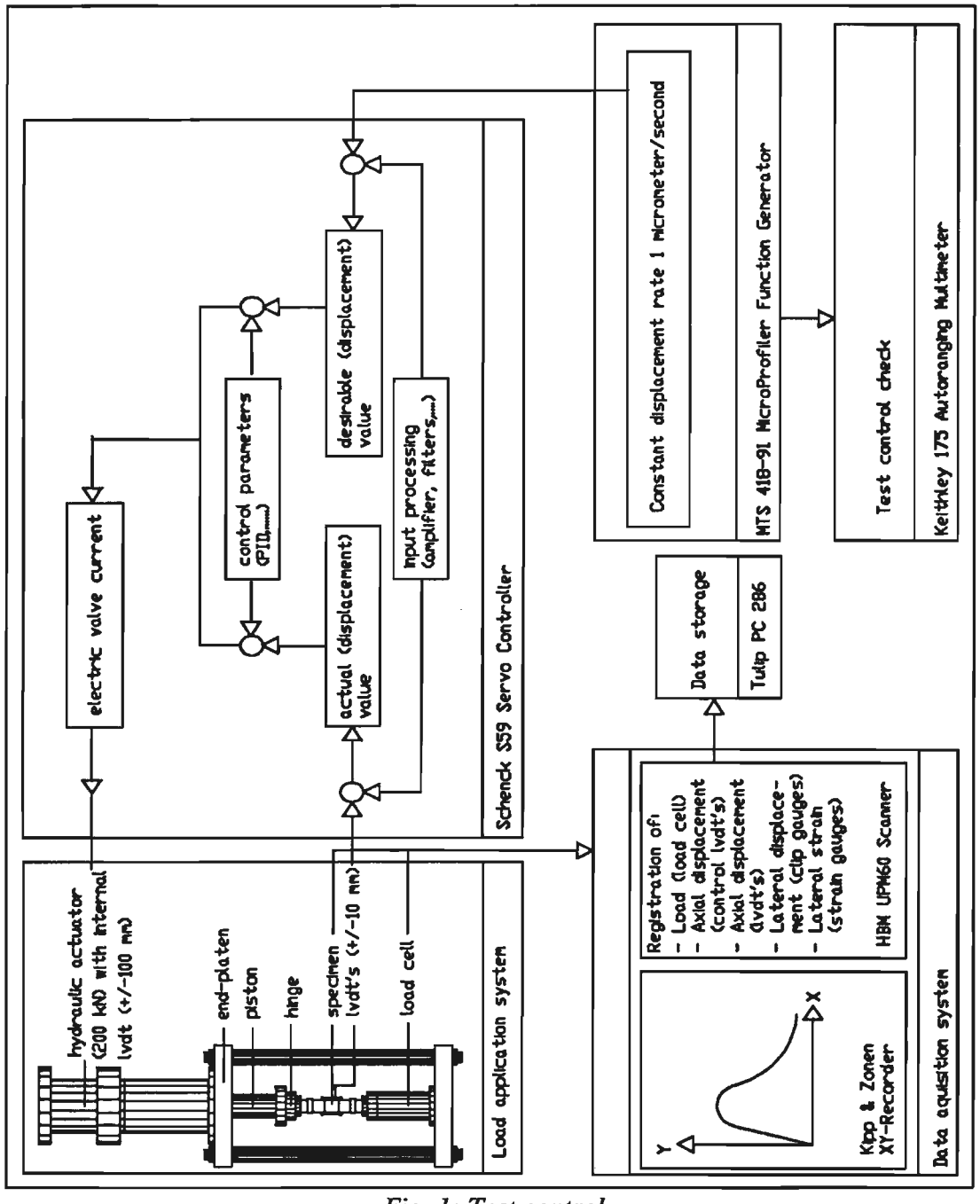

Fig. 1: Test control.

For testing concrete specimens of higher strength (and higher brittleness) with teflon platens, the axial displacement rate of 1 µm/s appeared to be an inappropriate test control, because of the very brittle post-peak behaviour. High strength concrete (200 mm high) specimens tested with this control parameter always failed in the postpeak region at about half the peak load. Therefore a different control parameter had to be used to registrate the whole descending branch of the stress-displacement curve.
One option is to use the lateral displacement as a feedback signal, but it was observed in normal strength concrete specimens that the clip gauges used for measuring this lateral displacement could fly off their seating and it was decided that the lateral displacement could in this case not be used as a control parameter.

Therefore a control parameter proposed by Rokugo et al. [1986] was applied, as indicated in fig. 2. Note that the control parameter given in fig. 2 is only correct for small values of θ (w'=w*cos(θ)-F*sin(θ)). By taking the control parameter as the axial displacement signal minus a portion of the axial force signal, the 'control axes' are rotated and in this respect no steep descending branch exists.

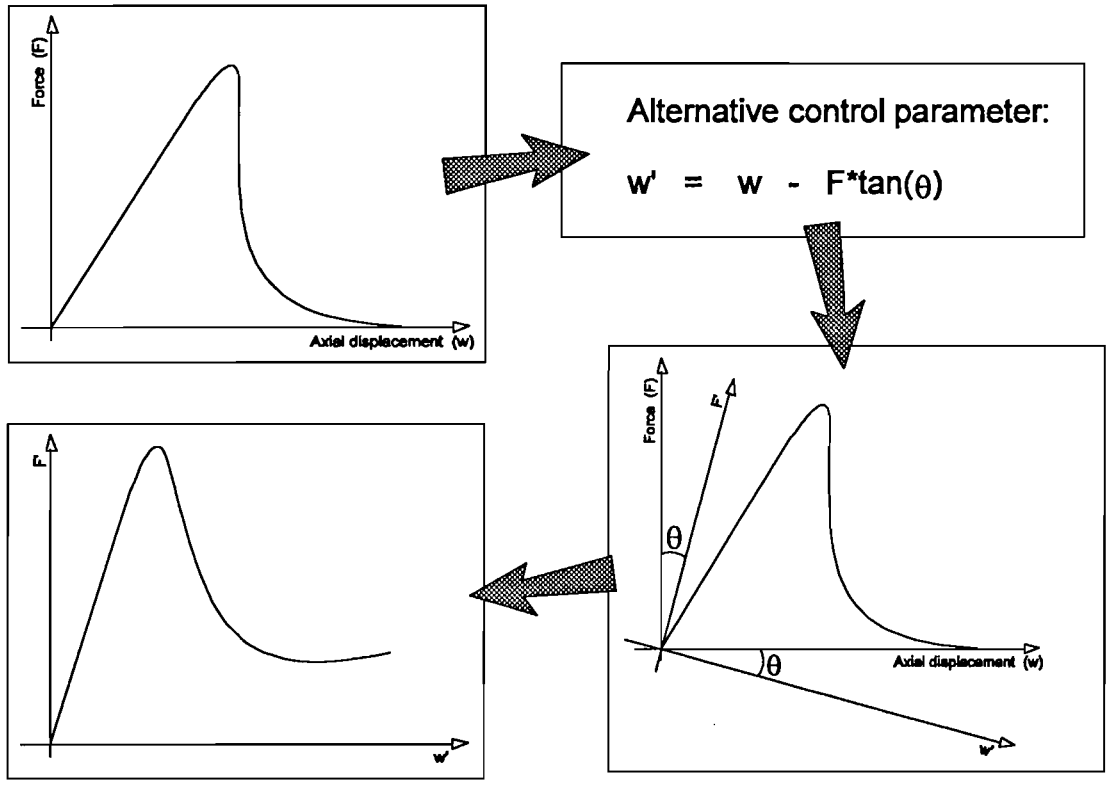

Fig. 2: Test control parameter for high strength concrete

2.3. Measuring technique.

2.3.1. Measurement of load and deformations.

The applied compressive force is measured by means of the load cell mentioned in §2.1. Axial deformations are measured in two ways:
1. One measuring channel registrates the average value of the two control-lvdt's (via the servo controller).
2. Four other channels record the axial deformations of four lvdt's, placed at the midsides of each of the specimen sides (thus two of them are located next to a control-lvdt), fig. 3a.
Lateral deformations are measured by means of clip gauges and strain gauges as indicated in fig. 3b. The lateral deformations are measured at three different heights: 10 mm below the top of the specimen, in the middle of the specimen and 10 mm above the bottom of the specimen. It would be preferable to measure all lateral deformations by means of clip gauges because strain gauges can not continue recording when larger cracks pass through them. However, for small specimen heights it is impossible to

mount three clip gauges above each other in two lateral directions. All lvdt's and clip gauges were recalibrated before starting the test program.

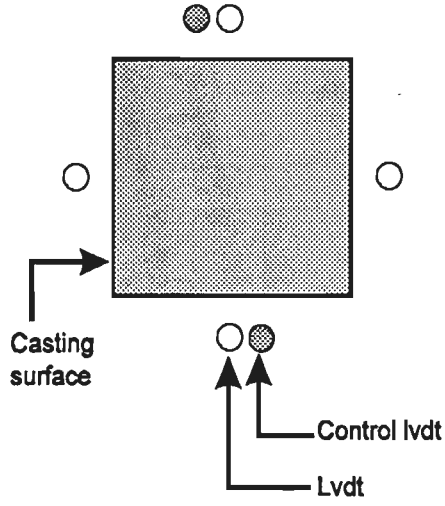

Fig. 3a: Measurement of axial deformations

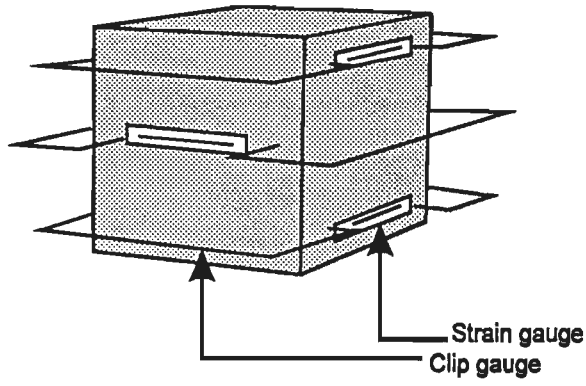

Fig. 3b: Measurement of lateral deformations

2.3.2. Data aquisition.

During a test the axial load-deformation diagram was plotted by a XY-recorder (manufacturer Kipp & Zonen). These diagrams were only used as a check on the numerical registrations and the stability of the test control. A HBM UPM60 Scanner was used to scan the several measurement channels. Software on a Tulip PC 286 forced the scanner to scan these channels every 5 seconds. Scanning occurred in the following order:

Channel 0	:	Load.
Channel 1	:	Average axial deformation of control-lvdt's.
Channel 2-7	:	Axial deformations of lvdt's.
Channel 8-13	:	Lateral deformations of clip gauges.
Channel 14-19	:	Lateral strain of strain gauges.

One measuring step took about 1 second.

2.3.3. Data handling.

In order to obtain the true axial displacement of the specimen, the measurements of axial displacement had to be corrected for two reasons:

- The measurements of the six lvdt's always show an initial setting, due to non-flatness of the concrete specimen and non-parallelness of the loading platen and the specimen.
- These measurements include the deformations of the loading platens.

The deformations of the loading platens were measured and a linear relation between force and loading platen deformation was assumed. No significant difference could be observed between the deformations of rigid steel platens and teflon platens (in fact the teflon platens showed a smaller slope in the linear relation). Therefore an average loading platen deformation correction was applied. After this correction the initial setting was eliminated as indicated in fig. 4. A different method was applied for high strength concrete because the ascending branch of the stress-displacement curve appeared to be quite linear (the upper and lower limit for curve fitting were determined by the required minimal r-square of the fit).

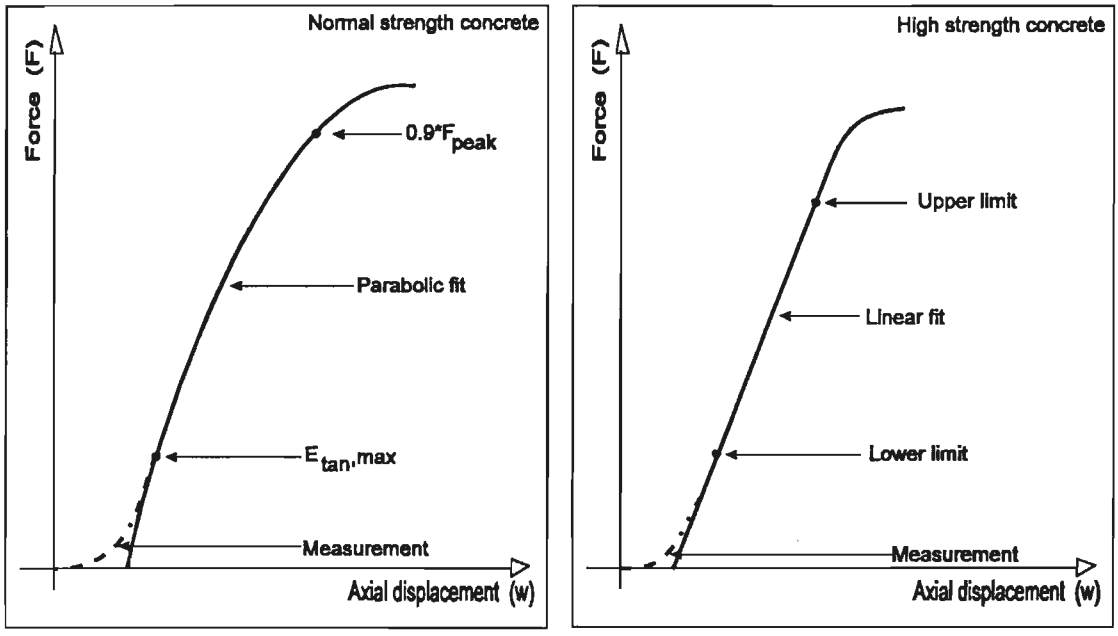

Fig. 4: Correction of initial setting in the stress-displacement curves

2.4. Reduction of lateral boundary restraint.

Besides tests with the polished steel platens mentioned in §2.1., tests were carried out using a friction reducing layer, consisting of a 0.05 mm teflon sheet separated from the steel platen by a very thin (µm's) layer of bearing grease (Molykote BR2 Plus). Frictional characteristics of both types of loading platens are similar to loading platens used by Vonk [1989a/b,1992]. Therefore no additional measurement of frictional properties was carried out, but the results of tests by Vonk are shown in appendix B.

The friction reducing layer was applied as follows. First, a small amount of grease was put in the center of the loading platen. Then with a tissue the grease was spreaded over the loading platen as uniform as possible. In this way excessive grease was also removed. Finally a sheet of teflon was placed upon the greased platen and air bells in between were rubbed out. The layer of grease was thin enough to be 'invisible', but thick enough to make the teflon stick firmly to the loading platen.

3. Test program.

3.1. Variations in specimens.

Two major variations were applied in the preparation of specimens:
1. A variation in size and shape. Three specimen heights were applied while maintaining a constant cross-section of 97*97 mm². These heights were 50, 100 and 200 mm and will be referred to as S (small), M (medium) and L (large) respectively. The cross-section of the specimens was determined by the size of the available loading platens.
2. A variation in concrete quality. Two different concrete qualities were applied as indicated in table 1.

Table 1: Concrete qualities (weight proportions)

		Normal Strength Concrete (N)	High Strength Concrete (H)
PC Cement Type B		15.8%	21.2%
Maximum aggregate size (Rounded river gravel)		8 mm	8 mm
Size distrib.	5-8 mm	17.0%	15.5%
	3-5 mm	5.7%	5.1%
	2-4 mm	15.3%	14.0%
	1-2 mm	11.5%	10.5%
	0.5-1 mm	11.5%	10.5%
	0.2-0.63 mm	9.8%	9.0%
	quartz sand	5.3%	4.9%
Admixtures		None	Microsilica 1.5%
Water/cement ratio		0.5	0.35 plus 0.5% superplasticizer

In fig. 4 the average results of two sieve tests from the same test sample is presented, compared with the sieve curve proposed by RILEM Committee 148ssc. The sieve tests were performed using Laboratory Test Sieves (manufacturer Endicott Ltd.).
Besides these variations other (not intended) variations occur:
1. Different positions of specimens in the original casting prisms. It is known (Van Mier, [1984b]) that specimens from end positions in casting prisms are better compacted on a vibration table than specimens from center positions. This phenomenon is caused by the difference in rigidity of the walls of the wooden mould at the center and at the end of the prism. At the center more vibration energy will be absorbed by the mould. Two precautions were taken to eliminate effects caused by this phenomenon on the test results as much as possible. Firstly, the moulds were stiffened with extra partitions. During compaction however it could be observed that even in these small moulds different compaction occurred at the different positions. Secondly, the effect was taken into consideration in the experimental design (§3.3.).

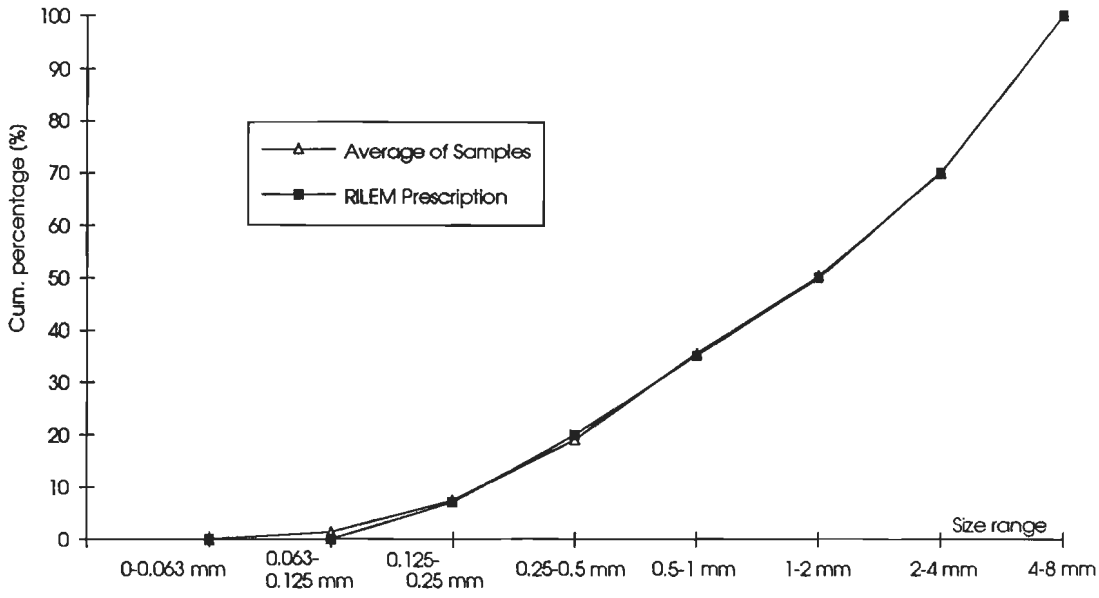

Fig. 4: Results of sieve tests.

2. Differences in batches. Because of the desired period between casting and testing (9 weeks) and the total testing time it was not possible to cast the specimens of one concrete quality in the same batch. Special attention has been paid to the composition of the mixtures of the several batches. In the experimental design it was decided to use 6 different batches: two for the normal strength concrete, two for the high strength concrete and one spare batch for each type of concrete. During casting it appeared necessary -with respect to the capacity of the mixing machine (Eirich SKG1 mixer, capacity 50 litres)- to cast each batch in two times (this means that in fact 12 batches were used).
3. Differences in specimen preparation. For several practical reasons it appeared impossible to obtain the same time scheme for all specimens. Especially the time needed for grinding the specimens was found to be a disturbing factor.

3.2. Specimen preparation.

In table 2 an overview is given of the initially desired specimen preparation procedure (per batch).

Table 2: Specimen preparation

Time:	Action:
1st day	Casting of 3 prisms and 5 cubes. Compacion by means of a vibration table (5 kHz) for about 45 (prisms) or 30 (cubes) seconds. Prisms and cubes covered with plastic, together with two bowls of water.
2nd day	Removing the bowls and covering the specimens with wet clothes.
After 2 days	Demoulding and putting prisms and cubes in water bassin of approximately 19-19.5 °C.

After 15 days	Sawing and grinding. Then placing specimens back in water bassin
After 28 days	Wiping specimens surface-dry and storage in sealed plastic bags
After 8 weeks and before 10 weeks	Testing

3.3. Experimental design.

In table 3 an overview is given of the original experimental design for the normal strength concrete only (the design for the high strength concrete is similar), in which both desired and undesired variations are considered. Specimens were cast in prisms of 150x150x450 mm^3, from which three specimens of different height could be sawn. With regard to the desired age of the specimens at testing and the time needed for carrying out a uniaxial compressive test, for both concrete types the specimens were cast in different batches as mentioned in §3.1. Specimens were sawn from the different batches as indicated in Appendix A.

Table 3.: Experimental design for concrete N showing all factors included

Specimen height	Batch	Prism position	Boundary Restraint	
			Rigid Steel Platen	Teflon Platen
50 mm	N1	End	N13SR	N12ST
		Center	N11SR	
	N2	End	N23SR	N22ST
		Center		N21ST
100 mm	N1	End	N12MR	N11MT
		Center		N13MT
	N2	End	N21MR	N22MT
		Center	N23MR	
200 mm	N1	End	N11LR	N13LT
		Center	N12LR	
	N2	End	N23LR	N21LT
		Center		N22LT

The specimens were coded as follows: The first character indicates the concrete type (N=normal strength concrete, H=high strength concrete), the second character indicates the batch (1, 2 or 3), the third character indicates the prism within this batch (1, 2 or 3, see Appendix A), the fourth character indicates the height of the specimen (S, M or L) and the last character indicates the type of the applied boundary condition during testing (R=rigid steel platen, T=teflon platen). For example: Specimen N23SR is a normal-strength specimen, sawn from prism 3 of batch 2, with a height of 50 mm (Small) and tested with rigid steel platens. Besides the 97x97 mm^2 specimens five 150 mm cubes were cast per batch to check the concrete quality by standard cube compression tests.

3.4. Actual test program.

In table 4 the actual test program is shown. All specimens were casted on day 1 and demoulded on day 3. The day of grinding lies somewhere between the day of sawing and the day of sealing.

Table 4: Actual test program

Specimen	Loading platen	Specimen height [mm]	Prism position	Sawing day	Sealing day	Testing day
Normal Strength Concrete						
N11SR	Rigid	50	Center	22	44	63
N13SR	Rigid	50	End	22	44	63
N32SR	Rigid	50	End	21	43	65
N12ST	Teflon	50	End	22	44	61
N21ST	Teflon	50	Center	22	38	65
N22ST	Teflon	50	End	22	38	65
N12MR	Rigid	100	End	22	44	64
N21MR	Rigid	100	End	22	38	64
N23MR	Rigid	100	Center	22	38	65
N11MT	Teflon	100	End	22	44	63
N13MT	Teflon	100	Center	22	44	64
N22MT	Teflon	100	End	22	38	65
N11LR	Rigid	200	End	22	35	64
N12LR	Rigid	200	Center	22	35	64
N23LR	Rigid	200	End	22	29	63
N13LT	Teflon	200	End	22	35	64
N21LT	Teflon	200	End	22	29	62
N22LT	Teflon	200	Center	22	29	63
High Strength Concrete						
H11SR	Rigid	50	Center	17	36	63
H13SR	Rigid	50	End	17	36	64
H32SR	Rigid	50	End	21	31	66
H22ST	Teflon	50	End	24	39	74
H23ST	Teflon	50	End	24	39	74
H31ST	Teflon	50	Center	21	31	66
H12MR	Rigid	100	End	17	36	69
H21MR	Rigid	100	End	23	39	72
H23MR	Rigid	100	Center	23	39	72
H31MT	Teflon	100	End	16	31	64
H32MT	Teflon	100	End	16	31	65
H33MT	Teflon	100	Center	16	31	65
H23LR	Rigid	200	End	31	39	72
H32LR	Rigid	200	Center	23	31	64
H33LR	Rigid	200	End	23	31	64
H11LT	Teflon	200	End	17	29	69
H13LT	Teflon	200	End	17	29	69
H21LT	Teflon	200	End	23	39	70
H31LT	Teflon	200	End	23	31	63

As can be seen from table 4, a large deviation from the original test program occurred for the high strength specimens, because a lot of specimens were used for trial test with the alternative test control described in §2.2.

3.5. Standard cube tests.

To get an impression of the concrete quality of the specimens, per batch five standard test cubes were cast. In table 5 the results of these standard compression tests are tabulated. The mean (standard) compressive strength of all concrete N cubes was 56.6 N/mm^2 (coëfficiënt of variation 6.2%, 14 tests). This value was found to be 80.8 N/mm^2 (coëfficiënt of variation 3.6%, 15 tests) for all concrete H cubes.

Table 5: Standard compression tests

Batch	Number of tests	Mean compressive strength (N/mm^2)	Variance (N/mm^2)	Coëfficiënt of variation (%)
N1	5	60.1	1.05	1.75
N2	4	57.2	1.07	1.87
N3	5	52.6	1.17	2.20
H1	5	80.9	2.61	3.22
H2	5	81.8	3.09	3.78
H3	5	79.8	3.22	4.04

4. Test results - Normal strength concrete.

Fig. 5a and 5b present the total of stress-strain curves for concrete N (18 tests). The size effect in softening is evident from these curves, under both boundary conditions. For smaller specimens the post-peak stress is higher at the same strain level. In the rigid platen tests a size effect on peak stress is observed. In the teflon tests this effect is much less clear. In the next section more comments will be made with respect to the size effect. In fig. 6a and 6b the curves are represented by stress-displacement curves.

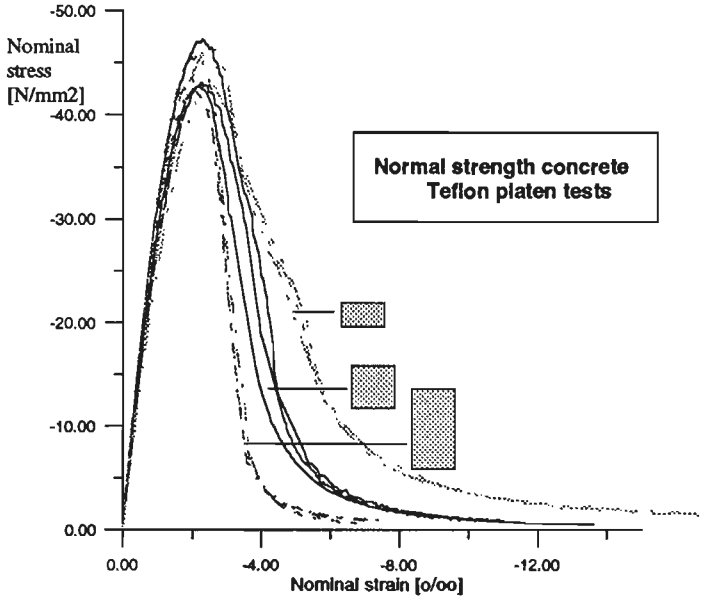

Fig. 5a: Stress-strain curves for Concrete N with Teflon platens

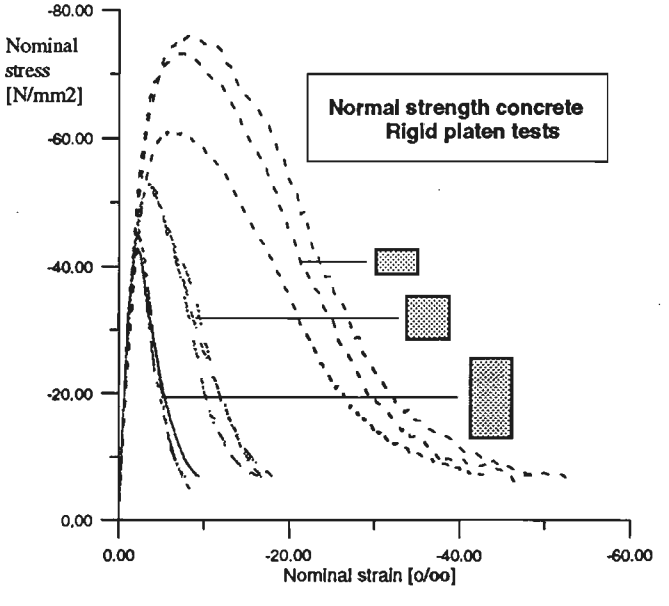

Fig. 5b: Stress-strain curves for Concrete N with Rigid platens

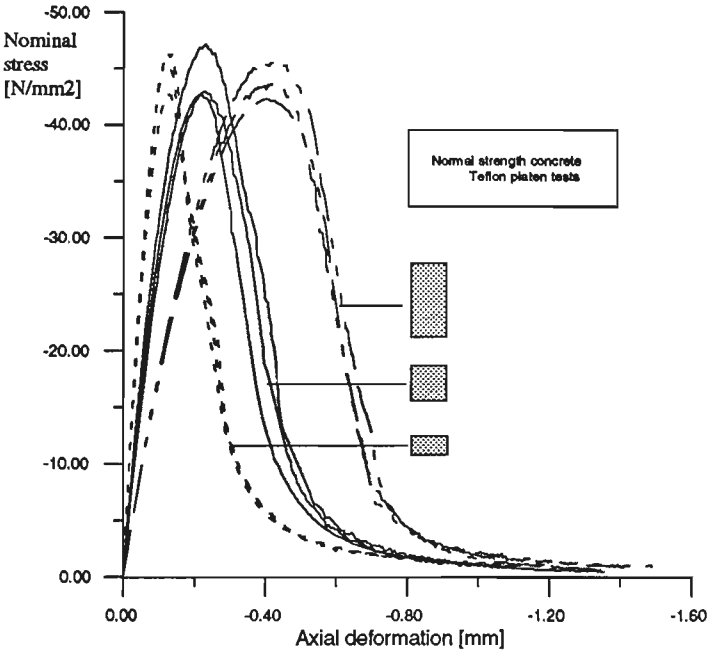

Fig. 6a: Stress-displacement curves for Concrete N with Teflon platens

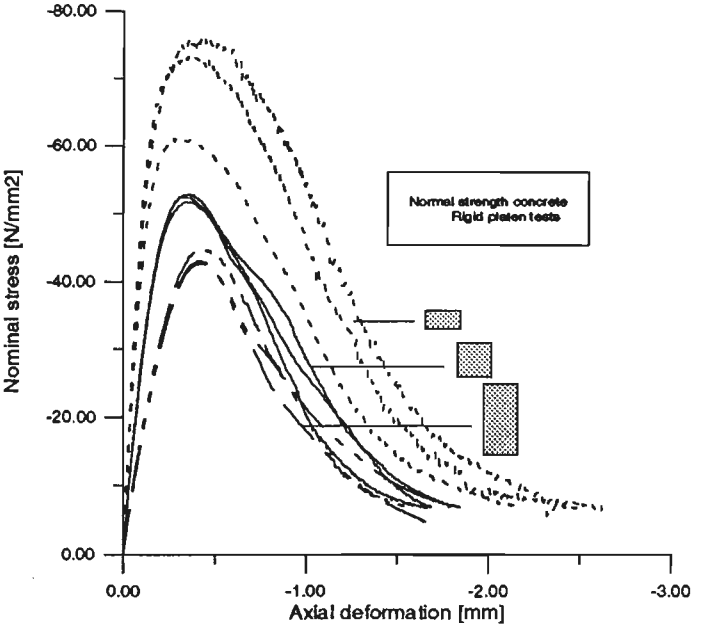

Fig. 6b: Stress-displacement curves for Concrete N with Rigid platens

4.1. Numerical results.

In table 6 several calculated results from the stress-strain (or displacement) curves are shown. A statistical analysis was performed using the program Statgraphics, available at the TU Eindhoven. The influence of differences in batches and differences in prism position was found to be not statistically significant. As could be expected, differences in height and boundary condition do have a statistically significant influence. It should be noted that influences of interactions could not be estimated (though it would be

possible to estimate some two-factor interactions in the original experimental design). In fig. 7 the difference between the fracture energies $G_{f,1}$ and $G_{f,2}$ is explained. Because $G_{f,2}$ (based on post-peak inelastic displacements) is the most realistic and most common representation of fracture energy, no further attention will be paid to $G_{f,1}$. The fracture energy for teflon platen tests was calculated up to -1.1 N/mm^2, for rigid platen tests up to -7.5 N/mm^2 in the descending branch of the axial stress-displacement curves.

Table 6: Calculated results for concrete N tests

specimen	E-mod. (N/mm^2)	$G_{f,1}$ per unit of area (Nmm/mm^2)	$G_{f,1}$ per unit of volume (Nmm/mm^3)	$G_{f,2}$ per unit of area (Nmm/mm^2)	$G_{f,2}$ per unit of volume (Nmm/mm^3)	Peak stress (N/mm^2)	Peak strain (o/oo)
N11SR	27307	73.044	1.4493	78.389	1.5553	-76.11	-8.26
N13SR	29735	64.7	1.2888	69.239	1.3793	-73.33	-7.7
N32SR	25045	55.647	1.1129	59.375	1.1875	-61.11	-5.48
N12ST	30725	7.728	0.1527	9.447	0.1867	-45.68	-2.28
N21ST	28554	6.818	0.1364	8.414	0.1683	-42.7	-2.44
N22ST	30679	7.339	0.1462	9.103	0.1813	-46.44	-2.4
N12MR	31576	39.471	0.3943	43.696	0.4365	-51.63	-3.45
N21MR	30133	37.757	0.3798	42.29	0.4255	-52.43	-3.28
N23MR	31246	32.334	0.3233	36.799	0.368	-52.82	-3.61
N11MT	30806	8.305	0.0831	11.305	0.113	-42.99	-2.27
N13MT	37280	9.31	0.0929	12.308	0.1228	-47.23	-2.3
N22MT	33750	7.698	0.0773	10.388	0.1043	-42.69	-2.11
N11LR	36288	25.088	0.1254	30.598	0.1529	-44.7	-2.205
N12LR	35034	28.361	0.1425	33.548	0.1686	-42.74	-2.2
N23LR	34621	25.083	0.1262	30.415	0.1531	-43.1	-2.055
N13LT	37365	10.047	0.0503	15.642	0.0783	-45.73	-2.155
N21LT	35983	9.973	0.0501	14.926	0.075	-42.31	-2.015
N22LT	36456	9.518	0.0479	14.71	0.074	-43.64	-2.08

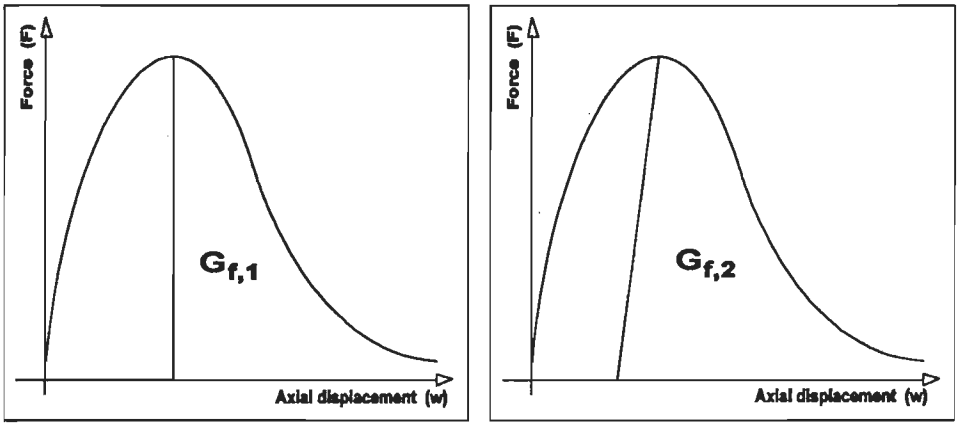

Fig. 7: Graphic representation of fracture energies in table 6

4.1.1. Pre-peak behaviour.

From the curves in fig. 5b (tests with rigid platens) it seems evident that there is a size effect in the pre-peak region. The higher the specimen, the lower the peak stress and strain. Rigid platens exhibit a very active boundary restraint, preventing deformations in the lateral directions. In smaller specimens the area in which a triaxial stress state occurs due to the boundary shear covers almost the entire specimen, which increases the maximum load and peak deformation tremendously. In the teflon tests this size effect on peak stress and strain is less pronounced but still present. The difference in peak stress between the 50 mm and the 200 mm high specimens is only 2.3%. It is not clear whether this (small) difference is mainly due to teflon friction or to a size effect as predicted by fracture mechanics. Some tests on specimens with the same shape but different dimensions could give more information about this. In fig. 8a and 8b the peak stress and peak strain are plotted against the specimen height.

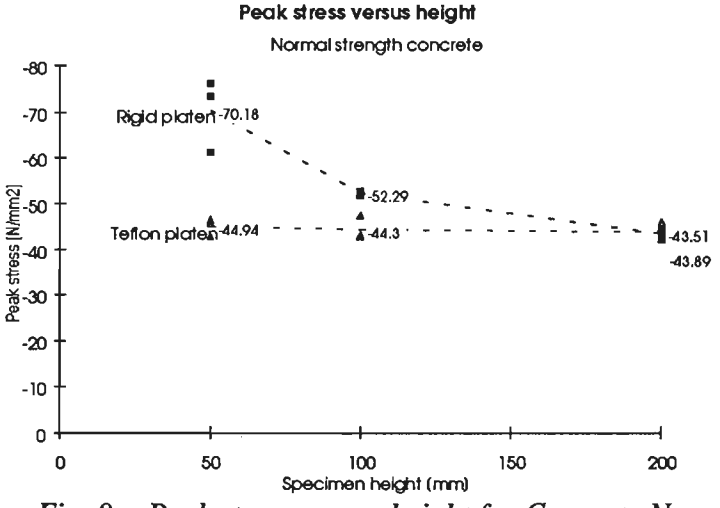

Fig. 8a: Peak stress versus height for Concrete N

From the tests it could be concluded that the size effect extends even into the Young's Modulus, but the values of this modulus calculated in table 6 appear to be quite sensitive to the method of calculating them (at which stress point). The average Young's Modulus from the tests was found to be 32366 N/mm^2 (calculated at 0.25 times the peak stress).

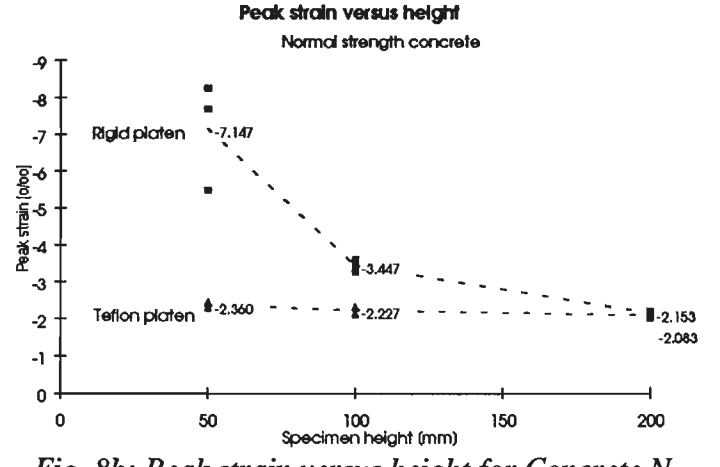

Fig. 8b: Peak strain versus height for Concrete N

4.1.2. Post-peak behaviour.

In fig. 9a and 9b the calculated fracture energy ($G_{f,2}$) is plotted against the specimen height (per area and per volume).

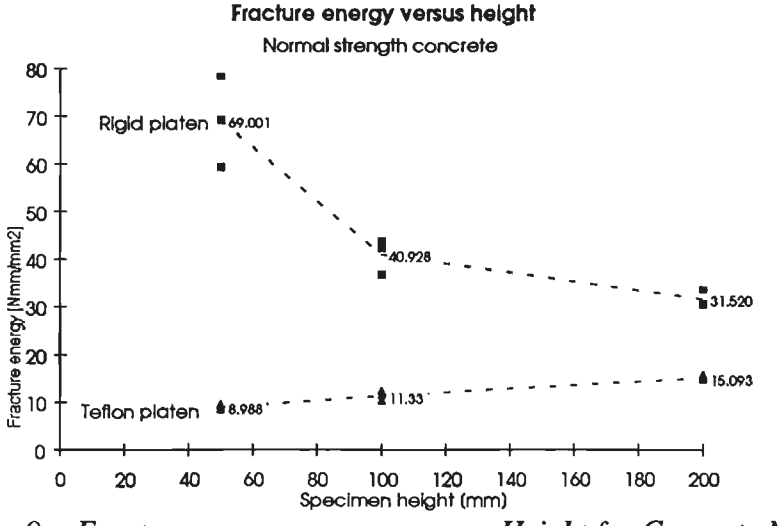

Fig. 9a: Fracture energy per area versus Height for Concrete N

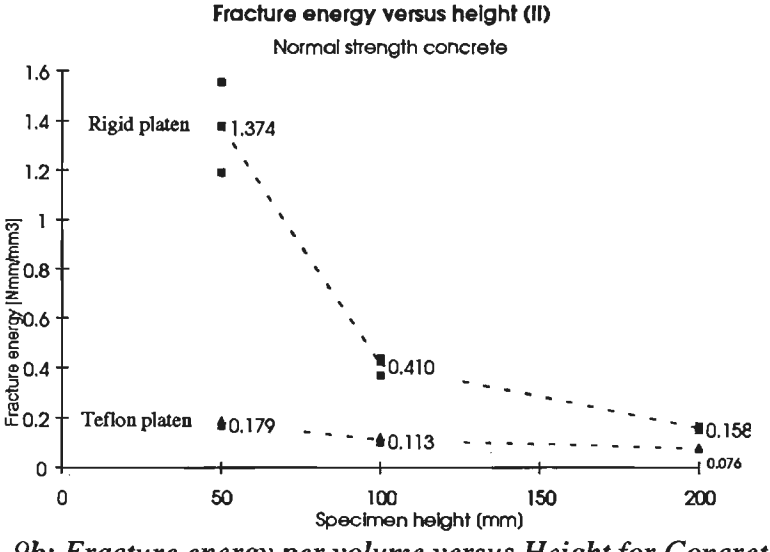

Fig. 9b: Fracture energy per volume versus Height for Concrete N

The teflon platen results shown in fig. 9a confirm the findings of Vonk [1992]: the softening proces is not a pure local (macrocrack) proces but also contains a contribution of the (microcracked) continuum part of the specimen. The continuum component becomes more important when the height of the specimen increases. This can also be observed in the (relative) stress versus (post-peak) displacement curves in fig. 10, where higher specimens show a larger post-peak displacement at the same relative stress.

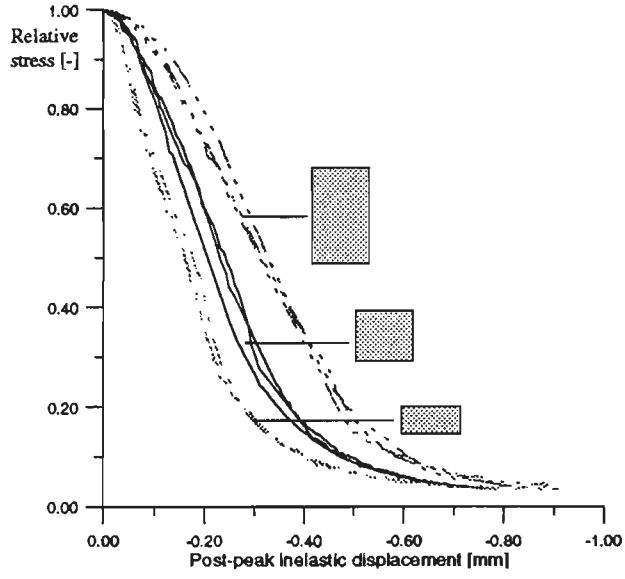

Fig. 10: Relative stress versus post-peak inelastic displacements for Teflon platen tests for Concrete N

In fig. 11 the calculated post-peak fracture energies from Vonk [1992] are plotted against the height for comparative reasons.

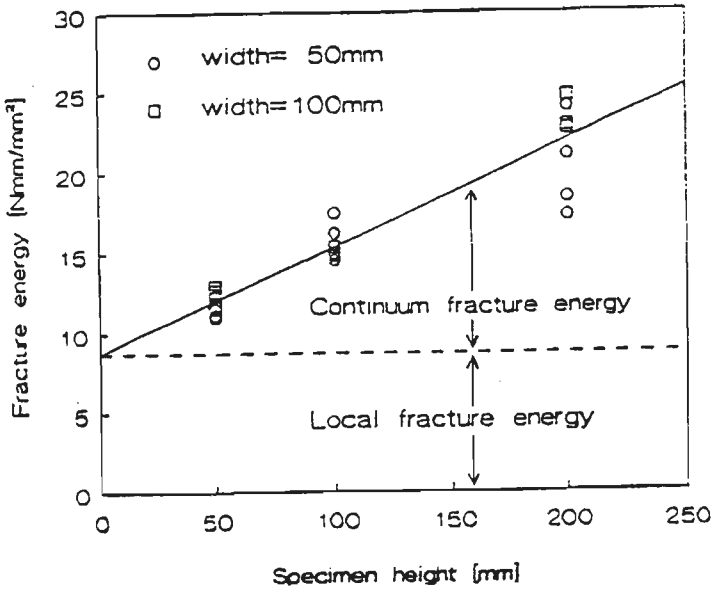

Fig. 11: Continuum- versus local fracture energies according to Vonk [1992]

The rigid platen tests do not give such a clear picture of the post-peak behaviour. Instead of an increase in fracture energy (per area) a decrease is observed with increasing specimen height. Because of the active boundary restraint not only the peak stress is higher for smaller specimens, but also the occurring axial deformations larger. In fact the term *fracture energy* becomes meaningless in this case. In fig. 12 the

(relative) stress versus (post-peak) displacement curves for the rigid platen tests are drawn.

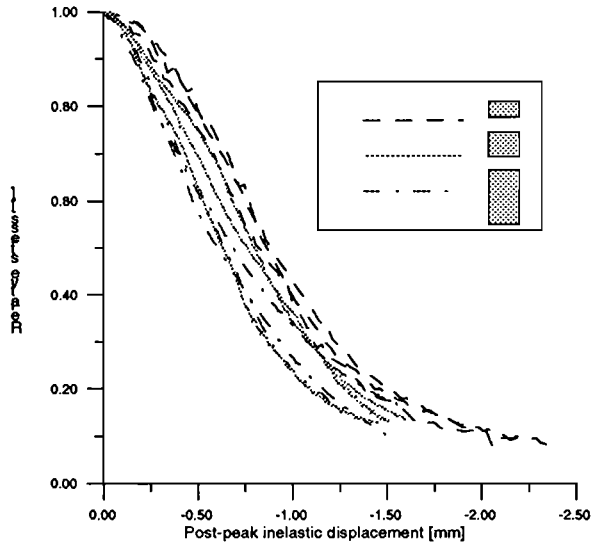

Fig. 12: Relative stress versus post-peak inelastic displacements for Rigid platen tests for Concrete N

4.2. Lateral boundary restraint.

From the stress-strain curves in fig. 5 the influence of the reduction of lateral boundary restraint is evident. The concrete behaviour in the rigid platen tests is so blurred by the influence of the boundary restraint that no reasonable conclusions can be deduced from them. In the teflon platen tests the 'real' concrete behaviour becomes more clear because of the very low frictional stresses at the loading platen-specimen boundary. For some tests an estimate was made of the external work by friction at this boundary, assuming that the frictional stress is equal to the axial stress times the coefficient of friction and that the displacements at the boundary -in total assumed equal to the lateral deformation at 10 mm from the specimen edge- show a linear variation over the boundary. The results were identical to the results of Vonk [1992]. See fig. 13. The frictional work is not negligible when compared to the calculated fracture energies, especially for smaller specimens (frictional work about 10% of fracture energy!). This indicates that the influence of lateral boundary restraint, even in tests with platens with low coefficients of friction like teflon platens, always blur the test results to some extent.

4.3. Localization and nonuniformity of deformations.

As shown by Bazant [1976] deformations tend to localize in the smallest volume possible because in that case the amount of energy required for failure is minimal. This means that a partial failure mechanism is preferred, sometimes resulting in a significant nonuniformity of deformations (rotation of the loaded boundaries).
From the lvdt-measurements in appendix C it is evident that for some tests a considerable rotation of the loaded boundaries occurs. It appears that -for teflon

platens- the rotation is larger for specimens of smaller height. It would be expected [Vonk, 1992] that the largest rotation is found for the highest specimens, due to the

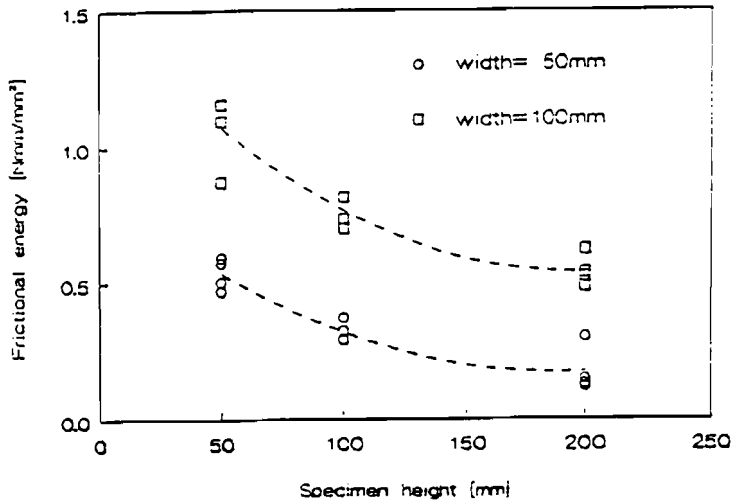

Fig. 13: External frictional work for several specimen geometries [Vonk, 1992]

more localized failure mode (see §4.5.). However, while the 'average' descending branch is indeed steeper for higher specimens, it is observed in the present tests that smaller specimens show a much higher gradient dσ/dw just after peak, immediately resulting in a considerable rotation. Following the analytical model of Vonk [1989c,1992] a more negative dσ/dw results in a larger rotation of the loaded boundaries according to:

$$\phi = \frac{-dbe\sigma + C\varphi_o}{C + \frac{db^3}{12}\left(\frac{d\sigma}{dw}\right)}$$

in which d and b are the specimen depth and width respectively, e is the eccentricity of the load, φ_0 the initial angle between specimen and loading platen surface and C the rotational stiffness of the loading apparatus. From the minimum value of dσ/dw (the steepest slope) in a test, the critical value of C can be determined following:

$$C_{critical} = -\frac{db^3}{12}\left(\frac{d\sigma}{dw}\right)_{critical}$$

With decreasing height dσ/dw becomes more negative resulting in a higher $C_{critical}$. As long as $C>C_{critical}$ no rotational instability will occur. In the present tests this condition was never satisfied, but in the case of large specimens (smallest $C_{critical}$) it seems that the rotational stiffness of the system was large enough to prevent a continuously increasing rotation. In figure 14 the rotational stifness of the system (specimen plus loading apparatus) is plotted against the axial deformation for three tests (N21ST, N11MT and N21LT).

It can be questioned if the observed rotation is significant with regard to the shape of the nominal stress-deformation curves. Only in the tests on small specimens (with teflon platens) a small 'bump' can be seen in the stress-displacement curves. More problems can be expected when testing high strength concrete.

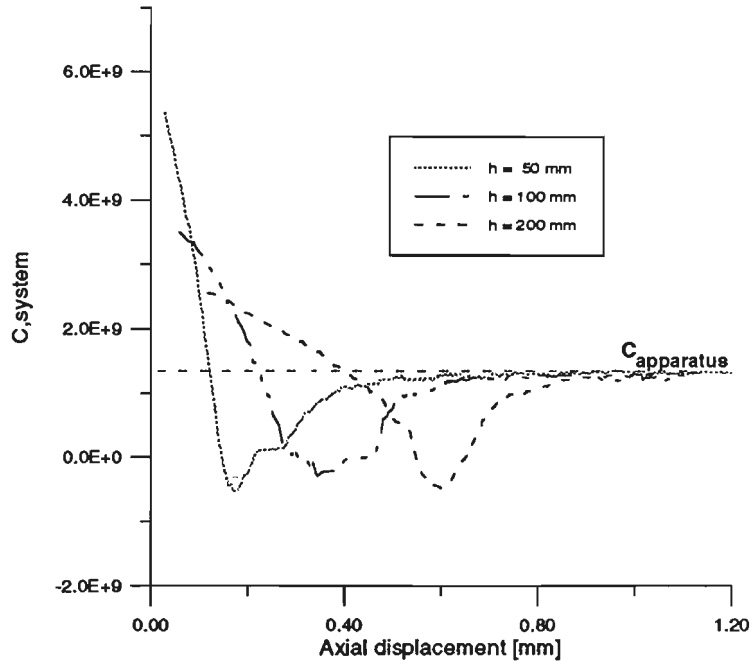

Fig. 14: Rotational stiffness of the system versus axial displacement

In the rigid platen tests, hardly any rotation of the loaded boundaries was found. This is due to the higher boundary restraint which has a stabilizing effect on softening and therefore prevents pronounced localization of deformations.

4.4. Lateral deformations.

In appendix D the lateral deformations measured by the clip gauges are plotted per specimen. For smaller specimens the scatter in clip gauge measurements is smaller than for higher specimens, both for rigid and teflon platen tests. This can be explained by the failure mode of the different specimens: smaller specimens show less localization of deformations and therefore a more uniform lateral displacement (see also [van Mier, 1984b]). The test results reject Vonk's hypothesis [1989a] that the rotation of the loaded boundaries is the most important factor causing the large scatter in lateral deformations. In the curves for the higher specimens in appendix D it can be seen which clip gauges crossed the localized (macro)cracks (large lateral deformation) and which clip gauges did not (small lateral deformation). For specimens loaded with rigid platens even at medium height a large scatter can be observed in clip gauge readings, because of the splitting off of large concrete pieces at the surface.
In appendix E the lateral deformations from both clip and strain gauges are plotted per specimen per side. Per specimen it is very clear at which side of the specimens (teflon platen tests) the onset of localisation of deformations occurred. Also the relatively uniform lateral expansion of specimens loaded with rigid platen tests is evident. Another observation that can be made from these figures is the uniformity of the lateral deformations measured at the different height positions on the specimens up to peak

stress for the teflon platens, being an indication for the effectiveness of the reduction of lateral boundary restraint of these teflon platens (see for example specimen N12ST). Note the 'snap-backs' which sometimes occur in the clip gauge measurements due to clip gauges flying off their seating.

4.5. Failure modes.

In figure 15 typical failure modes for the normal strength concrete specimens loaded with teflon platens are drawn. The macrocracks in all tests had an inclination with the loading direction of approximately 0 to 20°. It can be seen that for the highest specimens the localisation of deformations is more pronounced, resulting in just a few (usually one per side) macrocracks, most of them having an inclination of about 20°. For medium height specimens this inclination of cracks was almost the same, though the well-known 'zig-zag'-pattern of shear cracks was predominating. The small specimens were ruptured by a large amount of both vertical and inclined cracks and divided in a lot of small conical rest pieces (see also [van Mier, 1984b]).
All specimens (even the highest specimens) loaded with rigid platens failed according to the 'hour-glass'-failure mode, known from standard cube tests.
More illustrations of failure patterns can be found in Appendix F (photographs).

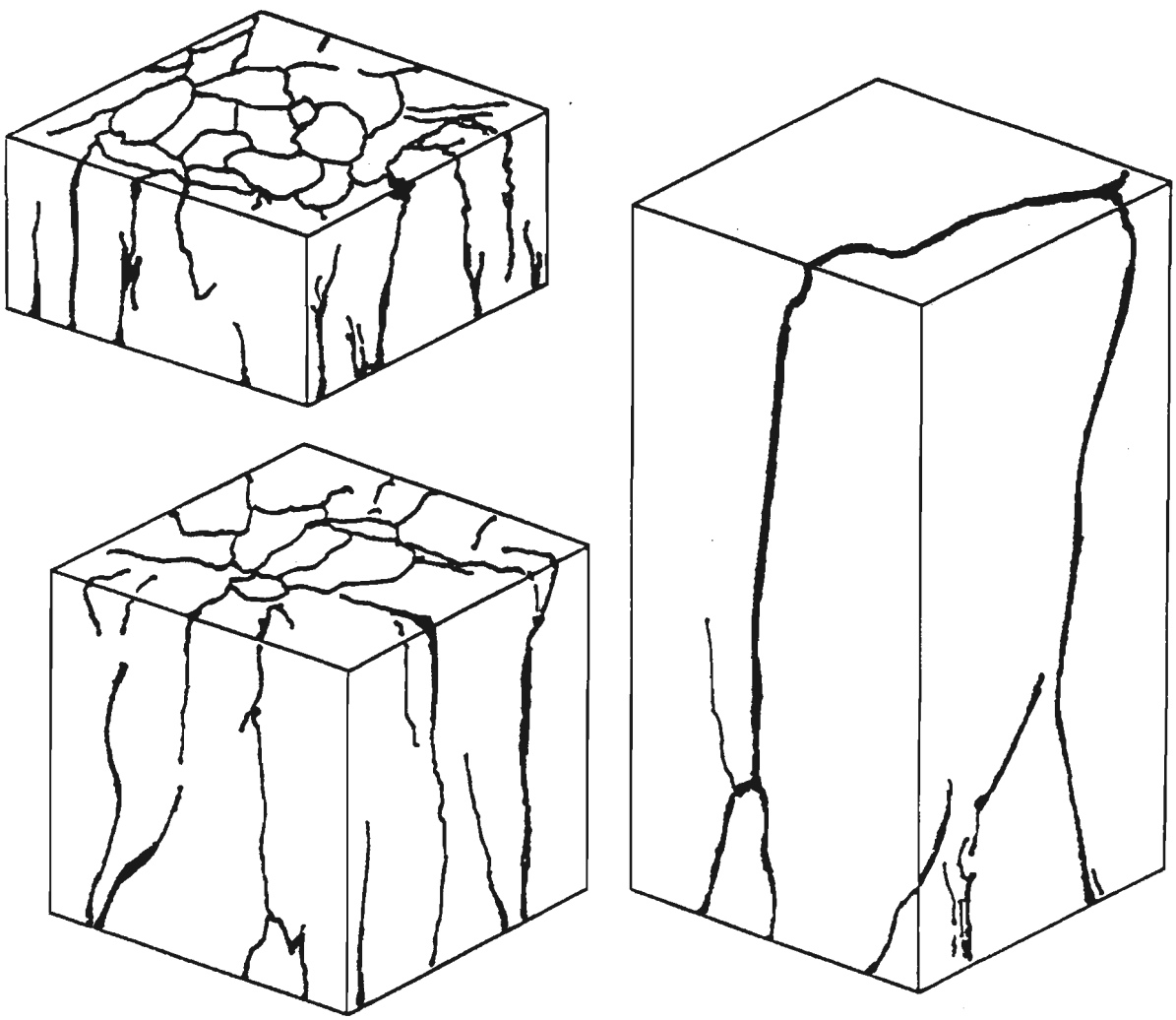

Fig. 15: Typical failure modes for normal strength concrete specimens (teflon tests)

5. Test results - High strength concrete.

In figures 16a and 16b stress-strain curves for all high strength concrete specimens are shown. It is not quite clear what causes the lower Young's modulus for the teflon platen tests on small specimens (fig. 14a). It is believed that it is a result of both test circumstances (it was for both concretes very difficult to obtain stable and reproducable results for small specimens, especially with rigid loading platens) and material behaviour. In fig. 17a and 17b the stress-displacement curves are plotted.

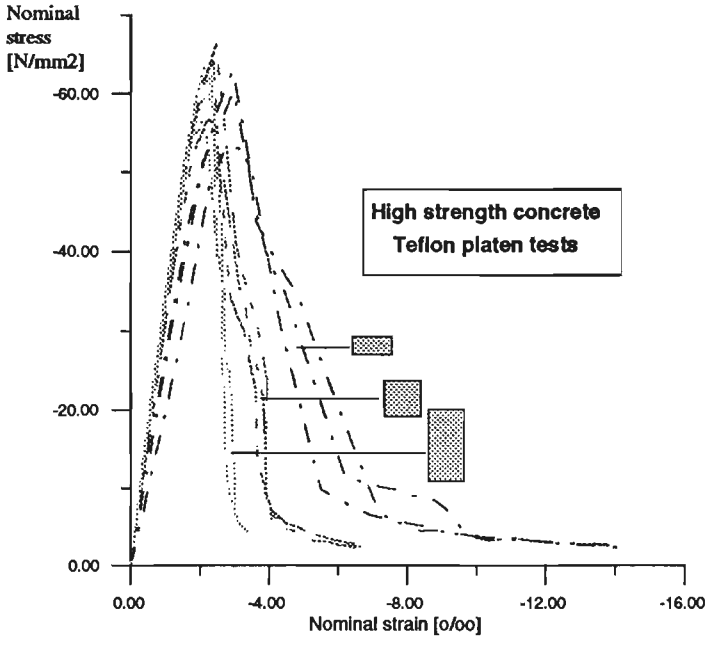

Fig. 16a: Stress-strain curves for Concrete H with Teflon Platens

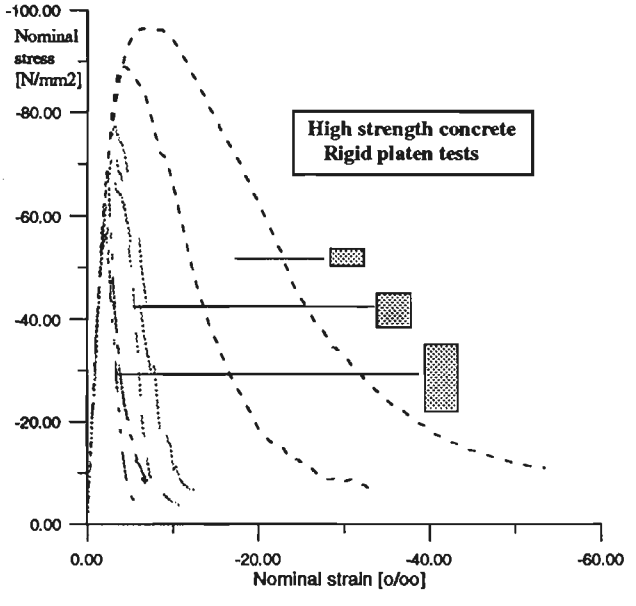

Fig. 16b: Stress-strain curves for Concrete H with Rigid platens

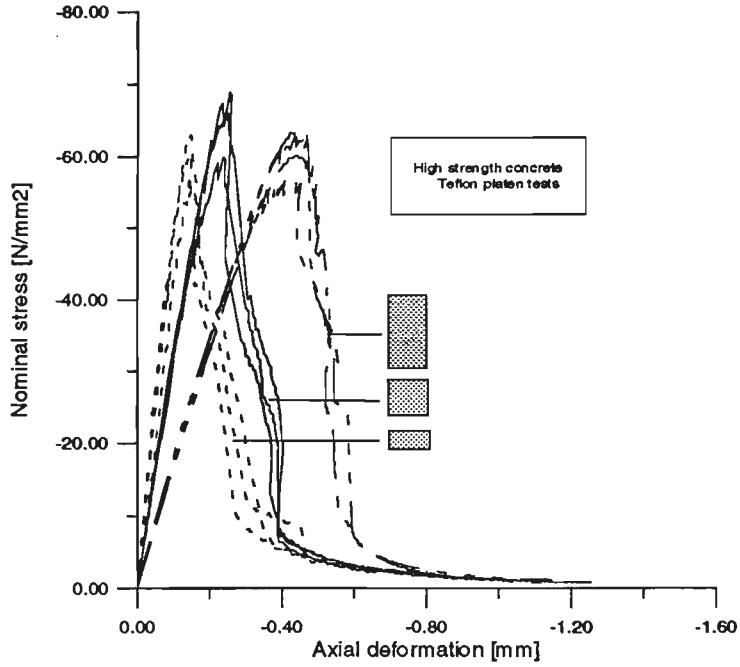

Fig. 17a: Stress-displacement curves for Concrete H with Teflon Platens

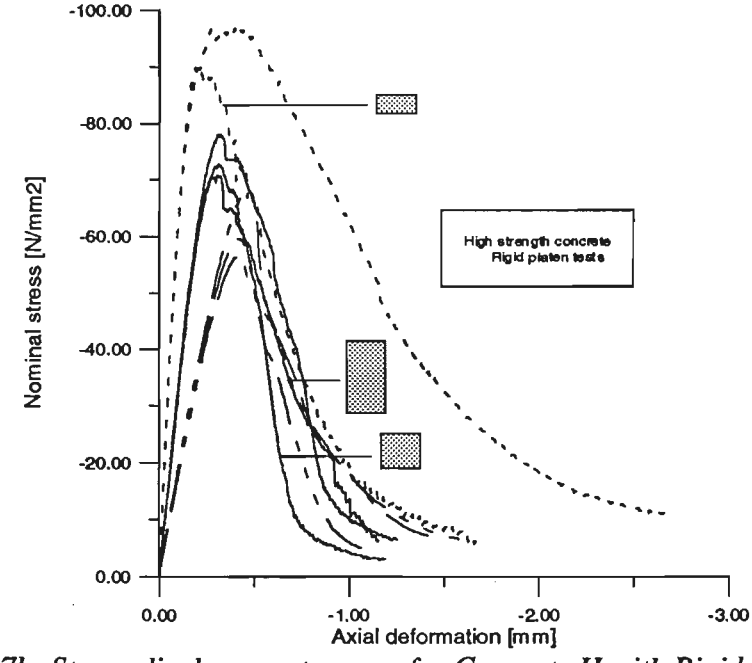

Fig. 17b: Stress-displacement curves for Concrete H with Rigid Platens

A size effect similar to the one for normal strength concrete can be observed, although the behaviour is more brittle. Peak stress and strain are higher than for normal strength concrete. The curves for specimen H11SR are omitted, because both peak stress and Young's modulus were extremely low (table 7).

The alternative test control (using a mixture of load and displacement signal as feed back signal) for teflon platen tests appeared to give satisfactory results, though the amount and size of 'control loops' in the stress-displacement curves are larger than in displacement control. An example of a force-displacement curve, recorded during testing by the xy-plotter, is shown in figure 18. Like in the tests performed by Rokugo

[1986], the larger control loops start with significant cracking, just before peak. The inclination of the loops is equal to the inclination of the alternative Y-axis. Because load and deformations were measured only once per five seconds the stress-strain curves in figure 16 give the impression that the test control was more instable than it actually was.

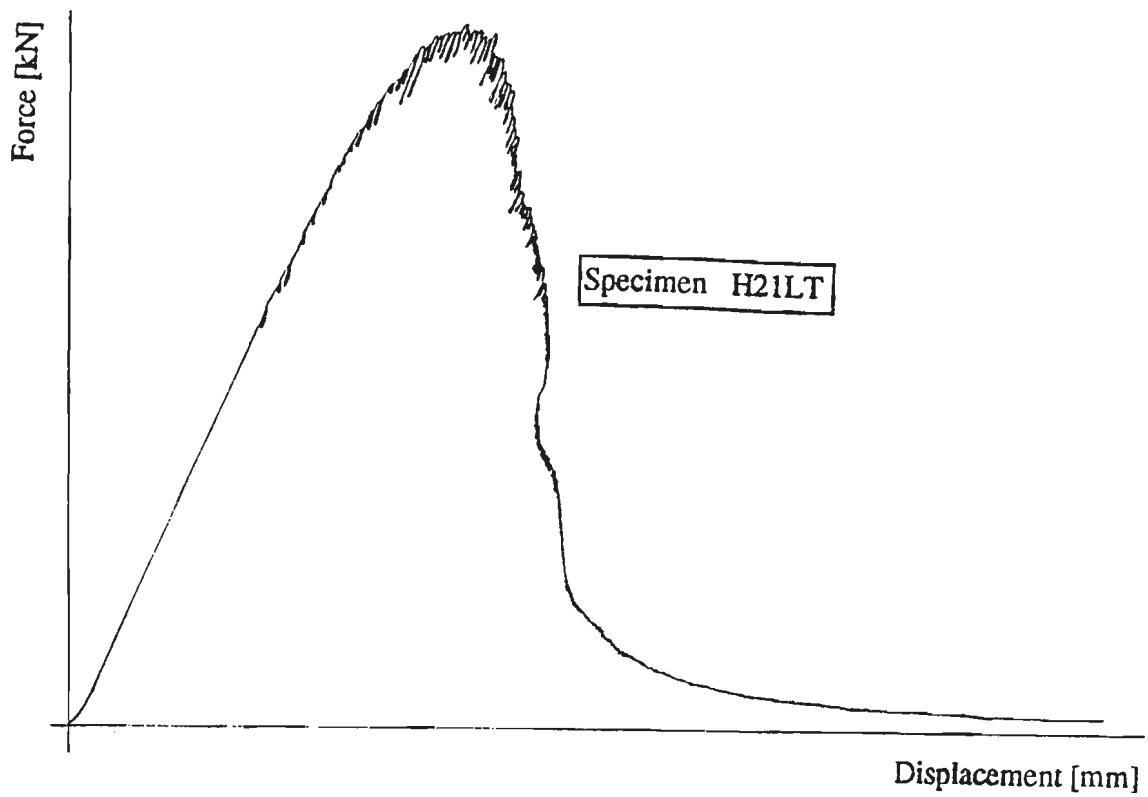

Fig. 18: XY-plot recorded during testing using the alternative test control

In figure 19 the difference between normal test control (displacement control) and the alternative test control is shown for the large high strength concrete specimens. The stress-strain curves seem to be identical up to peak stress. In the softening branch only the alternative test control provides a stable descending curve. It must be mentioned that -with the alternative control parameter- the loading rate before the peak was taken half the loading rate after peak, because the inclination of the alternative Y-axis was not much larger than the inclination of the ascending branch.

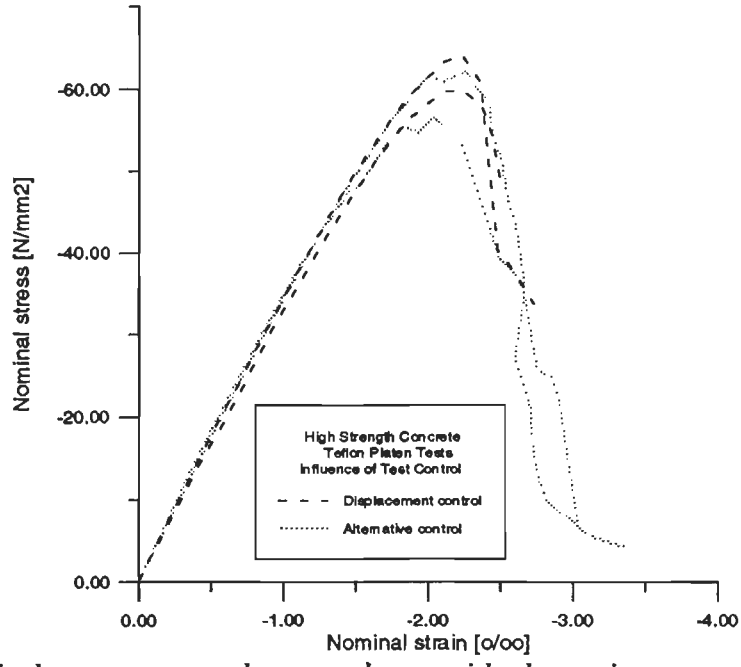

Fig. 19: Displacement control tests and tests with alternative control parameter

5.1. Numerical results.

Table 7: Calculated results for concrete H tests

Specimen	E-mod. (N/mm^2)	$G_{f,1}$ per unit of area (Nmm/mm^2)	$G_{f,1}$ per unit of volume (Nmm/mm^3)	$G_{f,2}$ per unit of area (Nmm/mm^2)	$G_{f,2}$ per unit of volume (Nmm/mm^3)	Peak stress (N/mm^2)	Peak strain (o/oo)
H11SR	22158	27.795	0.5581	32.551	0.6536	-65.06	-6.205
H13SR	36742	45.905	0.9090	51.491	1.0196	-90.16	-4.158
H32SR	35617	93.534	1.9527	99.845	2.0845	-96.88	-8.267
H22ST	25702	5.660	0.1116	9.573	0.1888	-62.99	-2.899
H23ST	28949	7.687	0.1540	10.832	0.2171	-60.41	-2.826
H31ST	19785	7.923	0.1563	12.037	0.2374	-56.67	-2.801
H12MR	33229	18.428	0.1843	26.389	0.2639	-72.74	-3.080
H21MR	32814	30.645	0.3065	39.919	0.3992	-78.01	-3.140
H23MR	34259	28.165	0.2786	35.572	0.3518	-70.85	-2.987
H31MT	34408	7.012	0.0701	13.411	0.1341	-66.36	-2.460
H32MT	32627	5.925	0.0589	11.457	0.1139	-59.90	-2.356
H33MT	33711	5.878	0.0584	12.958	0.1288	-68.88	-2.525
H23LR	38455	22.702	0.1134	34.755	0.1736	-68.05	-2.308
H32LR	35396	22.801	0.1142	31.842	0.1594	-56.61	-2.148
H33LR	36689	15.238	0.0763	24.892	0.1246	-59.55	-2.082
H11LT	33420	No fracture energies calculated				-60.15	-2.213
H13LT	35415	(Instable in displacement control)				-64.06	-2.239
H21LT	35181	6.640	0.0333	17.875	0.0896	-62.93	-2.179
H31LT	36878	8.011	0.0401	16.669	0.0835	-56.56	-2.039

In table 7 all calculated results from the high strength concrete tests are shown. Because of the large deviation from the original experimental design (see §3.4.) no useful statistical analysis could be performed on these results. Striking is the very large scatter in results for the small specimens loaded with rigid loading platens. Fracture energies were calculated up to -2.7 N/mm^2 for teflon platen tests and -15.0 N/mm^2 for rigid platen tests. The average Young's modulus was 33096 N/mm^2 (all test results).

In paragraphs 5.1.1. and 5.1.2. the pre- and post-peak behaviour of the high strength concrete are described. Because of the resemblance with the behaviour of normal strength concrete no additional comments are made with reference to the figures. In §5.2. a comparison is made with normal strength concrete.

5.1.1. Pre-peak behaviour.

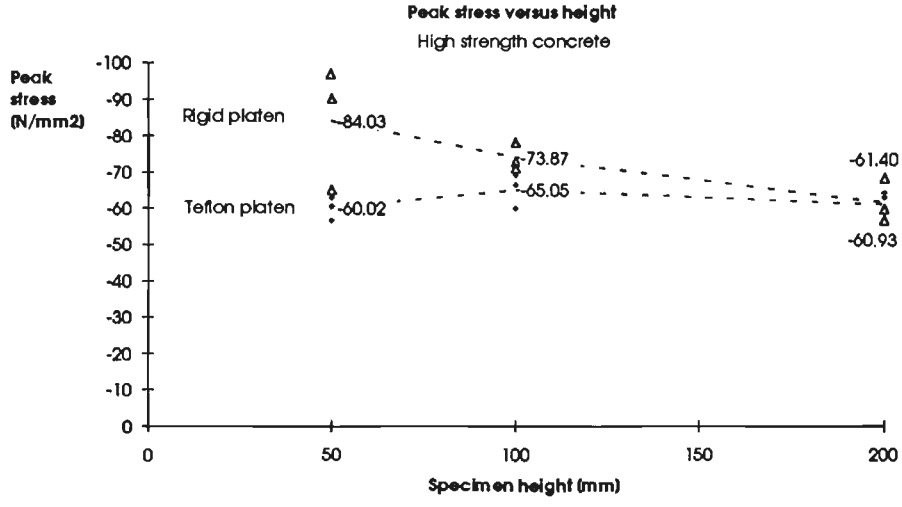

Fig. 20a: Peak stress versus Height for Concrete H

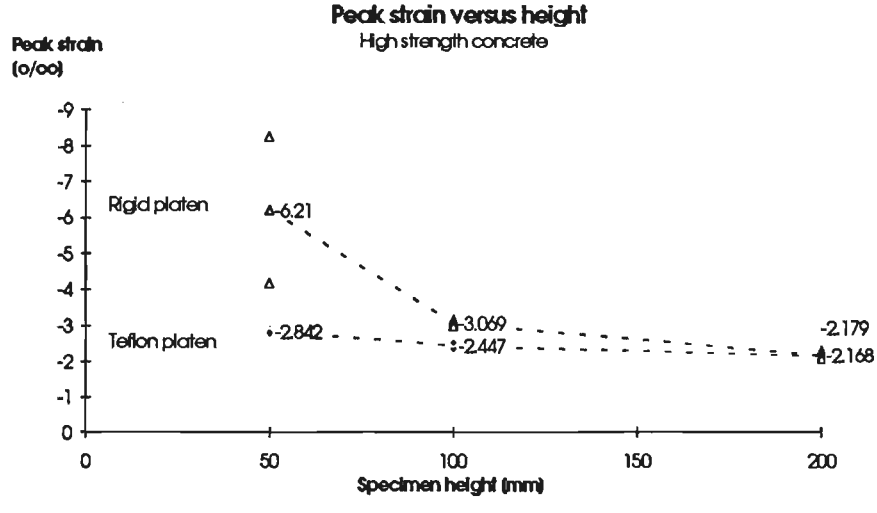

Fig. 20b: Peak strain versus Height for Concrete H

5.1.2. Post-peak behaviour.

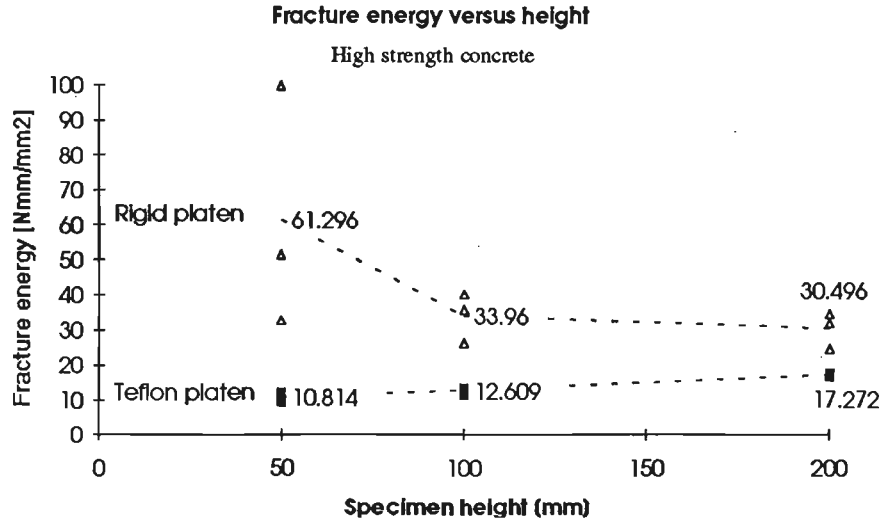

Fig. 21a: Fracture energy per area versus Height for Concrete H

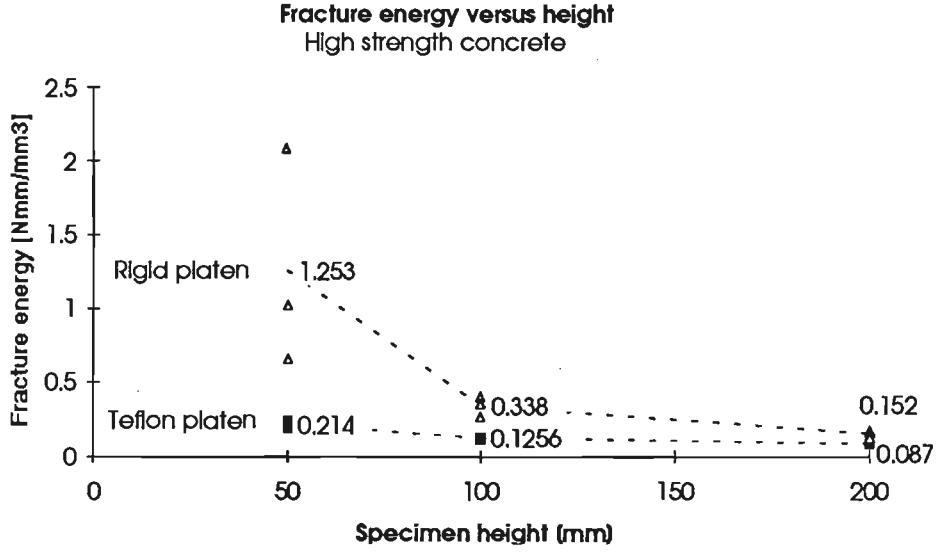

Fig. 21b: Fracture energy per volume versus Height for Concrete H

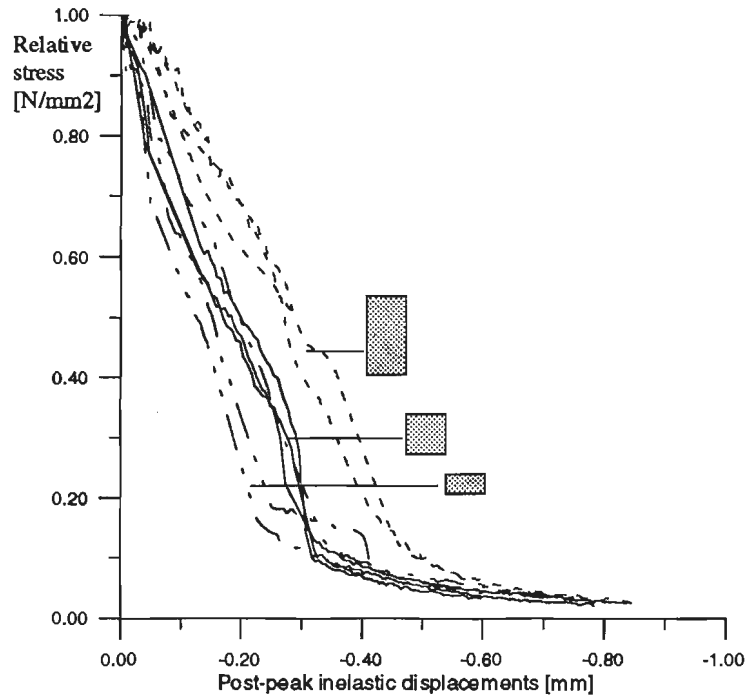

Fig. 22: Relative stress versus post-peak inelastic displacements for Teflon platen tests for Concrete H

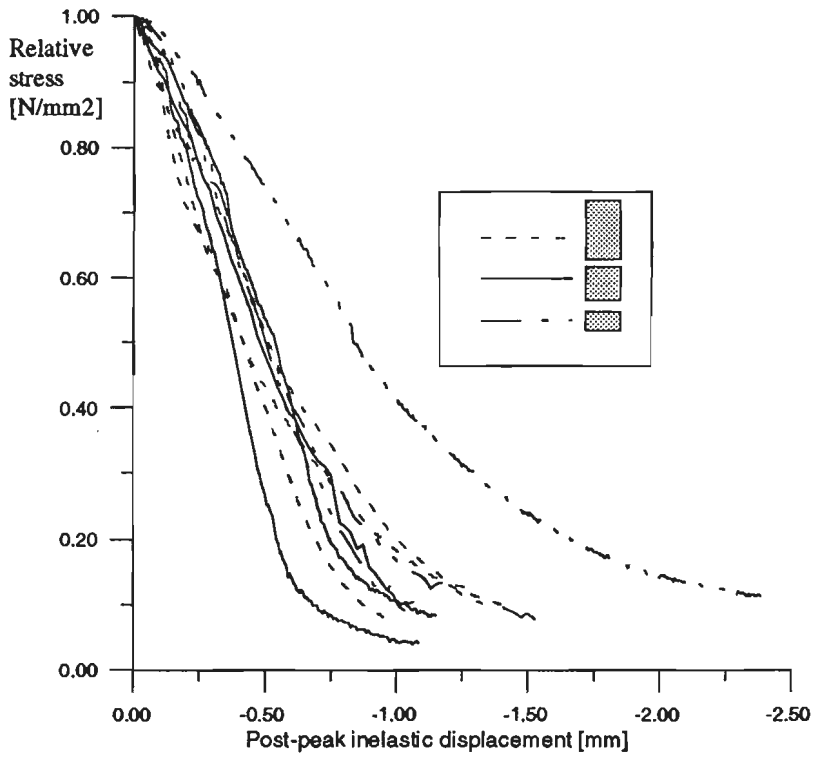

Fig. 23: Relative stress versus post-peak inelastic displacements for Rigid platen tests for Concrete H

5.2. Comparison with normal strength concrete

From the figures 20 through 23 it is obvious that -in a qualitative way of speaking- the behaviour of the high strength concrete does not differ from the normal strength concrete behaviour very much. The post-peak behaviour of the two types of concrete is compared in fig. 24, from which the difference in brittleness is evident. Note that care should be taken when interpreting fig. 24: the only real measure for brittleness is the slope of the descending branch of the nominal stress-strain curve.
No difference in crack patterns could be detected between the two concretes tested (figure 13). However, from the lvdt-measurements in Appendix C it can be concluded that a much larger nonuniformity of deformations occurs, due to the brittleness of the concrete, even for the large specimens. It seems that the testing of very brittle concretes like the high strength concrete tests in this report is beyond the reach of the loading apparatus. A loading apparatus with a higher stiffness would be better. Still it can be questioned what the influence of the nonuniform deformations is on the overall stress-displacement curves, compare for example the lvdt-measurements of H31MT and H33MT and their overall-curves.
Furthermore, the high brittleness of concrete H made a stable test control very difficult, leading to a larger variation in test results compared to the normal strength concrete, and a larger scatter in lateral deformation measurements (Appendices D and E). The curves in Appendix E indicate a strong influence of the direction of casting on the results. In nearly all high strength concrete tests fracture started at the casting surface, probably due to the poor workability of the concrete.

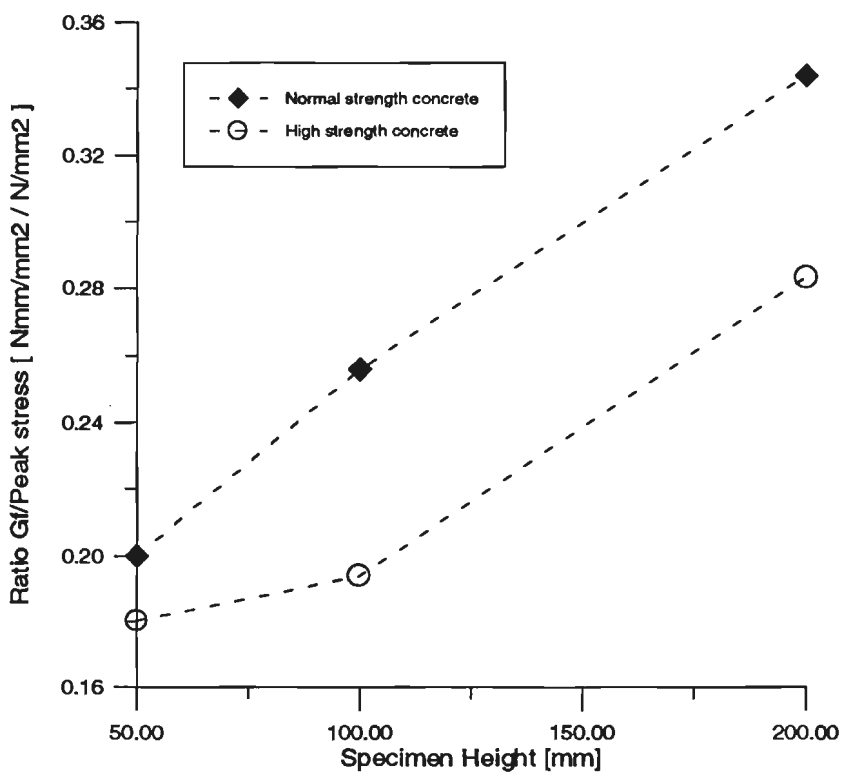

Fig. 24: Ratio Fracture energy/Peak stress for both concrete types

6. Conclusions.

From the tests results described in chapter 4 and 5 the following conclusions can be drawn:

1. In order to obtain reliable data regarding the softening behaviour of concrete in uniaxial compression, it is important to eliminate interfering effects from the test environment as much as possible, in particular friction between loading platen and specimen. When the friction at this contact surface increases, the behaviour of the material becomes more ductile. The teflon platens described in §2.4. perform quite well, though not all boundary friction is eliminated.

2. When the height of the specimen increases localization of deformations becomes more pronounced. However, due to the increasing continuum contribution to post-peak resistance the slope of the softening (stress-displacement) curve becomes less steep.

3. Peak stress and strain are found to decrease with increasing height, though the difference between 50 mm and 200 mm specimens is small. Considering the difference between the results from rigid and teflon platens, it could be assumed that -in the case of frictionless boundaries- no size effect on pre-peak results exists.

4. In a qualitative way of speaking no differences can be noticed between the tested normal and high strength concretes. Though exhibiting a more brittle behaviour, the high strength concrete displayed a similar response to changes in boundary friction or specimen size. Even the failure patterns appeared to be very much alike.

5. A large nonuniformity of deformations is observed for all teflon platen tests, with exception of large normal strength concrete specimens, indicating a lack of bending stiffness of the loading apparatus. (Uniaxial) testing of very brittle concretes (like the high strength concrete tests described in this report) seems to be beyond the reach of the loading apparatus. It still can be questioned to what extent the observed nonuniform deformations influence the average axial stress-displacement curves. Results from a loading apparatus with a higher bending stiffness are necessary to draw any conclusions.

Literature.

From research at the Eindhoven University of Technology:

1981 - VAN MIER, J.G.M., Multiaxial behaviour of concrete - Test methods and results, Survey of literature, Report Eindhoven University of Technology (in Dutch).

1984a - VAN MIER, J.G.M., Complete stress-strain behaviour and damaging status of concrete under multiaxial loading conditions, RILEM-CEB Symposium on Concrete under Multiaxial Conditions, INSA Toulouse, Session 3, Experimental results, V1, pp. 75-85.

1984b - VAN MIER, J.G.M., Strain-softening of concrete under multiaxial loading conditions, PhD Thesis, Eindhoven University of Technology.

1986a - VAN MIER, J.G.M., Multi-axial strain softening of concrete, part I: Fracture, part II: Load-histories, Materials and Structures, RILEM, V19, nr. 111, pp. 179-200.

1986b - VAN MIER, J.G.M., Fracture of concrete under complex stress, HERON, V31, nr. 3.

1988 - VONK, R.A., GOUDSWAARD, I., A detection method for internal cracks in concrete specimens, Report Eindhoven University of Technology (in Dutch).

1989a - VONK, R.A., Influence of boundary conditions on softening of concrete loaded in compression, Report Eindhoven University of Technology.

1989b - VONK, R.A., RUTTEN, H.S., VAN MIER, J.G.M., FIJNEMAN, H.J., Influence of boundary conditions on softening of concrete loaded in compression, Fracture of Concrete and Rock: Recent Developments, eds. S.P. Shah, S.E. Swartz and B. Barr, Elsevier Applied Science, London, pp. 771-720.

1989c - VONK, R.A., Uniformity of deformations in compression tests on concrete, Report Eindhoven University of Technology.

1990a - VONK, R.A., Constitutive model describing interface behaviour with tensile and shear softening, Report Eindhoven University of Technology.

1990b - VONK, R.A., RUTTEN, H.S., VAN MIER, J.G.M., FIJNEMAN, H.J., Size effect in softening of concrete loaded in compression, Fracture Behaviour and Design of Materials and Structures, ed. D. Firrao, EMAS, UK, pp. 767-772.

1991 - VONK, R.A., RUTTEN, H.S., VAN MIER, J.G.M., FIJNEMAN, H.J., Micromechanical simulation of concrete softening, Fracture Processes in Concrete, Rock and Ceramics, eds. J.G.M. van Mier, J.G. Rots and A. Bakker, RILEM Proceedings 13, E & FN Spon, London, pp. 129-138.

1992 - VONK, R.A., Softening of concrete loaded in compression, PhD Thesis, Eindhoven University of Technology.

1992 - BONGERS, J.P.W., Concrete behaviour under multiaxial loading conditions - Modelling in a finite element package, Graduate Thesis, Eindhoven University of Technology.

1993 - STYS, D., Influence of the microstructure on the strain softening of concrete under compression, Report Eindhoven University of Technology.

1994a- BONGERS, J.P.W., RUTTEN, H.S., VAN MIER J.G.M., FIJNEMAN, H.J., Softening behaviour of concrete loaded in multiaxial compression, Computer Modelling of Concrete and Structures, Proceedings EURO-C 1994 International Conference, Innsbruck, Austria, pp. 302-312.

1994b- BONGERS, J.P.W., Constitutive models describing concrete continuum and local material behaviour, Report Eindhoven University of Technology.

From other research:

1976 - BAZANT, Z.P., Instability, ductility, and size effect in strain-softening concrete, Journal of the Engineering Mechanics Division, Proc. ASCE, V.102, nr. EM2, 1976, pp. 331-334.

1986 - ROKUGO, K., OHNO, S., KOYANAGI, W., Automatical measuring system of load-displacement curves including post-failure region of concrete specimens, Fracture toughness and fracture energy of concrete, ed. F.H. Wittmann, Elsevier Science Publishers B.V., Amsterdam, pp. 403-411.